University of Tehran

Earth Observation and Geomatics Engineering

Online ISSN: 2588-4360

Homepage: https://eoge.ut.ac.ir/

A Dual-Layer UAV Workflow for Tree-Level Monitoring of Tree Decline Using RGB Imagery and a Lightweight Deep Learning

(Selected Paper in the 8th ISPRS Geospatial Conference 2025, University of Tehran, Iran)

Marziye Ghasemi [1,2], **Hooman Latifi** [3✉]

1. Dept. of Photogrammetry and Remote Sensing, Faculty of Geodesy and Geomatics Engineering, K. N. Toosi University of Technology, Tehran-Iran. E-mail: mrzghasemi@email.kntu.ac.ir
2. Dept of Civil Engineering, Iran University of Science & Technology, Tehran-Iran
3. Corresponding author, Dept. of Photogrammetry and Remote Sensing, Faculty of Geodesy and Geomatics Engineering, K. N. Toosi University of Technology, Tehran-Iran. E-mail: hooman.latifi@kntu.ac.ir

Article Info

Article type: Original papers
Research Article

Article history:
Received 2026-01-18
Received in revised form 2026-01-28
Accepted 2026-01-28
Available online 2026-06-02

Keywords:
Dual-Layer UAV,
Point cloud,
Tree decline,
PDI,
DAI.

ABSTRACT

Tree decline is a serious multifaceted problem in Zagros forests of Iran. The prevalence of this complex phenomenon in the recent decades highlights the need for high-resolution geospatial monitoring approaches. While unmanned aerial vehicle (UAV)-based photogrammetry offers a flexible and cost-effective means of capturing forest health, conventional top-of-canopy imaging fails to sufficiently represent critical under canopy features, including stem morphology and lower crown structure that is commonly prone to early symptoms of tree decline.

We presented a dual-layer UAV photogrammetric framework that combines above- and below-canopy imagery to detect phenotypic decline in *Quercus brantii* using a novel 3d tree reconstruction method followed by a MobileNetV2 deep learning model to detect decline symptoms on stems. Using this detection, we computed the Phenotypic Decline Index (PDI) and Decline Acuteness Index (DAI) to describe decline severity and trends in continuous form. The MobileNetV2 achieved overall classification accuracy of 96.3% (F1-score = 0.94) in distinguishing healthy and declined stems (n = 299). This performance, derived from a confusion matrix with 166 true positives, 9 false negatives, 11 false positives, and 133 true negatives, highlights the model's high reliability. Furthermore, the UAV-derived DAI correlated strongly with multi-year field-based decline trajectories (Pearson r = 0.718, Spearman ρ = 0.928), confirming the method's reliability.

Decline severities during three years of field data collection followed by suggested consistent shift amongst levels of tree decline, while UAV-based phenotypic analysis was shown to enable capturing nuanced changes in tree vitality. By yielding high correlations, we provide a cost-effective and high-resolution workflow for phenotyping oak decline, which enables multi-scale analysis of structural and symptomatic indicators using RGB-only data.

Cite this article: Ghasemi, M., & Latifi, H. (2025). A dual-layer UAV workflow for tree-level monitoring of tree decline using RGB imagery and a lightweight deep learning. *Earth Observation and Geomatics Engineering*, Volume 9, Issue 2, Pages 93-102. http//doi.org/10.22059/eoge.2026.409794.1206

Publisher: University of Tehran.
DOI: http//doi.org/10.22059/eoge.2026.409794.1206

1. Introduction

Forest ecosystems worldwide are facing threats caused by climate change and human activities (Finch et al., 2021), in particular in arid, semi-arid, and other fragile ecosystems. A particular example is Iran´s semi-arid Zagros forests with a semi-Mediterranean climate that encompass an area of ca. 6 million ha, i.e., 44% of the total forest area in Iran (Sagheb Talebi et al., 2014). Oak decline in Zagros manifests as a complex interaction of abiotic and biotic stressors, with *Quercus brantii* Lindl. (Brant's or Persian oak) as the predominantly affected species. Field studies have documented a progression from initial crown dieback (65% trees affected initially) to more than 50% canopy loss in 80% of monitored trees within four years, which directly correlates with reduced leaf area and photosynthetic capacity (Gallardo-Salazar et al., 2023). In-depth knowledge of the location of the decline-affected areas and, in turn, the spatial representation of decline severity is among the main priorities for an improved understanding of tree decline, which leads to management decisions for their protection and conservation, pest treatment, and forest stand restoration (Imanyfar et al., 2019).

Traditional field-based monitoring (e.g. manual crown transparency assessment, dendrometric measurements) faces severe scalability constraints in Zagros' rugged terrain, capturing less than 0.1% of trees due to accessibility challenges (Fekry et al., 2022). Additionally, field-based sampling and data collection are also laborious, time- and cost-intensive as well as possibly destructive.

Geospatial data and methods introduce convenient alternatives. As tree decline syndrome in areas associated with increased non-photosynthetic vegetation can contribute to increased reflection in visible domain, decreased reflection in the NIR domain, and increased ground temperature due to lack of plant transpiration (Huang et al., 2018), large regional coverage data can be paired with active and passive satellite data to enable tracking tree decline (Mantas et al., 2022). However, various challenges were reported when applying space borne remote sensing data, with the main challenge being the limited spatial resolution, which contributes to background effects on reflection (Zarco-Tejada et al., 2019) in case of low- and medium-resolution data. In comparison, high spatial resolution data such as Rapid Eye (Zakeri Anaraki and Fallah Shamsi, 2014) and Worldview (Navarro-Cerrillo et al., 2019) provide better means to analyze the decline severity. However, their use is constrained by their high costs, limited availability, and the fact that it is not possible to detect single crowns even at 1-m pixel size (Dash et al., 2017). Satellite-based methods (e.g., Landsat NDVI) lack granularity to detect individual tree symptoms, with more than 30% error in sparse canopies (Meddens and Hicke, 2014). While single tree measurements are amongst the most basic components of forest inventory, yet they form the basis of our understanding of the forested areas of the world (Magnuson, 2024). While providing structural accuracy (vertical precision: 2–3 cm) and canopy penetration by LiDAR systems, it fails to capture spectral symptoms of decline (bark lesions, rosiness) specially on stem basis (Fekry et al., 2022).

Recent progresses in unmanned aerial vehicles (UAVs) photogrammetry enabled leveraging high-resolution, three-dimensional data for detailed assessment of forest structure and health (Xiang et al., 2019). These techniques offer a cost-effective and flexible alternative to traditional field-based or expensive LiDAR-based surveys (Myronenko and Song, 2010), which are often limited by terrain complexity, instrumentation costs, and logistic constraints in remote environments. While conventional UAV photogrammetry relies solely on above-canopy imagery, it misses critical sub-canopy indicators of decline progression (Ghasemi et al., 2022) due to occlusion effects. This limitation restricts it's ability to capture critical sub-canopy features such as stem geometry and lower crown morphology (Wang et al., 2021b; Olson et al., 2025). Recent attempts to address this issue have explored multi-layer UAV data integration, but several limitations still persist. For instance, prior studies using combined above- and under-canopy UAV laser scanning have improved stem visibility and Diameter at breast height (DBH) estimation accuracy (Wang et al., 2021a). However, these methods rely on expensive LiDAR systems and often require complex hardware setups, restricting their accessibility for forest inventory routines. Moreover, LiDAR-derived point clouds inherently lack spectral or textural information (e.g. RGB, multispectral information), which are critical for assessing tree health indicators such as canopy discoloration or bark texture anomalies. Recent innovations have demonstrated photogrammetry's cost-effectiveness for 3D forest modelling, particularly when integrated with machine learning (Table 1).

Critically, existing approaches discretize decline severity into arbitrary classes (e.g., healthy/moderate/severe), obscuring its inherently continuous nature. This categorical simplification impedes early detection of incipient decline and quantitative tracking of intervention efficacy (Finch et al., 2021).

The Phenotypic Decline Index (PDI) and the Decline Acuteness Index (DAI) introduced by Finch et al (2021) represent significant methodological leaps by continuously integrating structural (crown volume, height-diameter ratio) and symptomatic (transparency, stem decline signs) variables through percentile ranking. However, these indices traditionally depend on field data collection (Finch et al., 2021), constraining spatial scalability. This paper proposes a new method that overcomes this limitation through a dual layer UAV photogrammetric pipeline that automates input variable acquisition across the entire decline continuum.

Here, we introduce an integrated UAV photogrammetric workflow to address critical limitations in monitoring oak decline on *Q. brantii* trees within Iran's semi-arid Zagros forests in western Iran. We aim to: 1) develop a dual-layer (above/below-canopy) flight strategy capturing

complementary structural and descriptive data inaccessible to conventional remote sensing, 2) implement MobileNetV2-based detection of stem decline symptoms using sub-canopy imagery, 3) quantify crown transparency as a continuous variable via 3D ray marching and 4) automate calculation of continuous decline indices (PDI/DAI) by integrating these UAV-derived variables. Our approach overcomes LiDAR's inability to resolve spectral biomarkers and replaces discrete severity classifications with a physiologically grounded continuum, enabling scalable, high-resolution assessment of decline trajectories across heterogeneous forests.

Table 1. Comparative summary of methodical capabilities for tree decline monitoring.

Technology	Structural Accuracy	Spectral Resolution	Stem Symptom Detection
Terrestrial LiDAR	±1 cm	Limited (intensity)	Poor
Nadir UAV Photogrammetry	±5–10 cm	High (RGB)	None (occluded canopy)
Our Dual-Layer UAV	±3–8 cm	Very High (RGB + texture)	Excellent (direct imaging)

2. Materials and Methods

This study operationalizes the established PDI and DAI framework to assess Q. brantii decline in Iran's Zagros forests. While retaining the core index formulations, we introduce novel descriptors optimized for Zagros oak ecosystems. PDI quantifies current decline severity, whereas DAI captures temporal decline rates (Finch et al., 2021). Both indices require integrated structural and phenotypic data from entire tree architectures, which are unattainable via conventional aerial photogrammetry.

To achieve comprehensive 3D reconstruction, we implemented a Dual-Layer UAV flight strategy, where the resulting images further proceed in a photogrammetry-based workflow (Figure1). The products are PDI and DAI, which were computed by synthesizing: 3D structural feature, crown decline percentages, stem decline signs and crown transparency.

2.1. Study Area

Data were collected from two permanent plots (A and B) within a representative semi-arid region of Iran's Zagros Mountains. This area, characterized by an average annual temperature of 13.7°C and precipitation of 522 mm, is ecologically significant for its flora, fauna, and non-wood forest products, with *Q. brantii* as the keystone species (Chaharmahal and Bakhtiari Administration, 2025). The forests face degradation from anthropogenic pressures (unsustainable harvesting, overgrazing, land-use change, poor silviculture) disrupting natural regeneration, compounded by climate stressors like drought, pests, and other pathogens creating deteriorating phenomena like charcoal decease (Sagheb Talebi et al., 2014; Pourhashemi and Sadeghi, 2020). UAV data acquisition was conducted using three flights per plot: above-canopy (Phantom 4 Pro), and below-canopy at low (DJI Tello) and high (DJI Mavic Pro) resolutions. Each plot contained 100 mature oak trees; field dendrometric variables (DBH, Diameter at Root Collar (DRC), tree height and crown dimensions) and geolocations were sourced from the Research Institute of Forests and Rangelands (RIFR) inventory database.

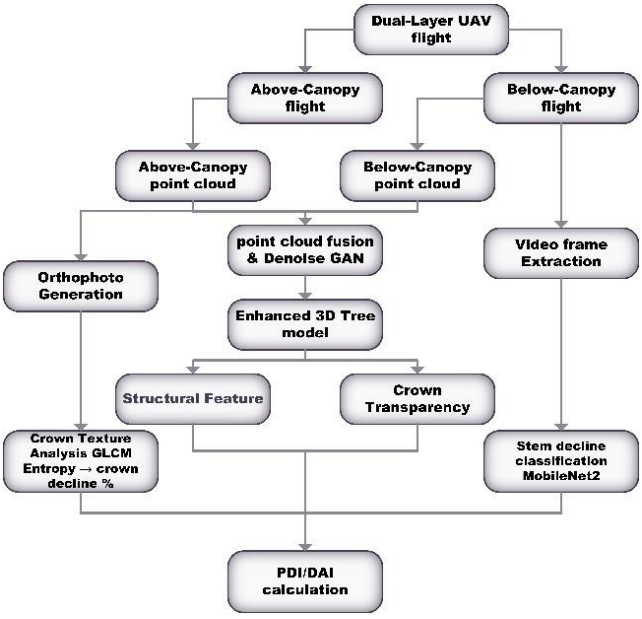

Figure 1. workflow of proposed Method.

2.2. Data

Field data collection occurred in September 2024 across both sample plots. Three primary datasets were acquired:

1.Above-canopy UAV imagery: Collected using a DJI Phantom 4 Pro (20 MP CMOS sensor, 8.8 mm lens, 84° FOV) flown at 80 m altitude in cross-grid mode. Each plot was imaged in two missions: nadir and 60° oblique, with 80% longitudinal/lateral overlap. Flights were conducted at early morning (Plot A) and afternoon (Plot B), pre-programmed via PIX4D capture Pro.

2.Below-canopy UAV imagery: Manually flown within tree clusters (6-10 trees) using two platforms:

Low-Resolution (DJI Tello): Selected for programmability (3 flights: 2 in Plot A, 1 in Plot B; 5 MP, 25 mm lens, 82.6° FOV).

High-Resolution (DJI Mavic Pro): Selected for image quality (4 flights: 2x per plot; 12.35 MP, 26 mm lens, 78.8°

FOV). Videos were recorded in closed-loop paths around tree groups.

3.Ground Control Points (GCPs): Six GCPs per plot (corners and center points) were surveyed using a RayMand Iro Pro II GPS receiver via RTK connected to the national "Shamim" network for georeferencing.

Validation utilized field-measured tree structural attributes (DBH, DRC, height, crown) and decline severity as 4 class severity explanation by experts in field collected in 2018-2020, assuming negligible growth-related changes in these slow-growing oaks.

2.3. Pre-Processing

Above-canopy imagery underwent initial quality control, discarding frames with motion blur, shadows, noise, or insufficient overlap. Retained images were processed in Agisoft Metashape Pro 2.2.0 using Structure-from-Motion (SfM) to generate a dense point cloud, georeferenced to real-world coordinates using surveyed GCPs, ensuring metric accuracy across the entire plot. Below-canopy video frames were extracted, screened for instability artifacts (take off/landing/sudden motion), and similarly processed via SfM in Agisoft Metashape. However, the below-canopy point clouds remained in local coordinate systems due to limited GCP visibility under the canopy. These clouds provided detailed reconstructions of proximal objects but exhibited sparse, noisy background features due to limited parallax and inconsistent appearance, as confirmed by depth maps during alignment.

To generate complete 3D tree models, the locally-coordinated below-canopy point clouds (derived from un-georeferenced video frames) were fused with the georeferenced above-canopy point cloud using a novel geometric method. This method identifies corresponding tree positions (using angles and relative distances) to compute similarity transformation parameters, aligning the below-canopy data within the above-canopy coordinate system (Ghasemi et al., 2025). The resulting fused point cloud per tree, while spatially aligned, remained noisy and sparse. It was subsequently enhanced using a novel, unsupervised Generative Adversarial Network called Denoise_GAN. Denoise_GAN directly processes raw photogrammetric point clouds without requiring labelled training data. It progressively removes noise and outliers (while preserving crown/stem macrostructure) and prioritizes stem diameter gradients and crown expansion patterns through shifted convolutional layers. This approach overcomes key limitations of existing methods in semi-arid forests, specifically the reliance on ground patterns (often bare during data collection) for matching, the need for large training datasets, overlap requirements, and sensitivity to scale differences between above/below-canopy acquisitions and inherent photogrammetric noise. Denoise_GAN enables scalable 3D reconstruction without LiDAR infrastructure or extensive labelled data (Ghasemi et al., 2025).

2.4. Measurement of Tee Structural Attributes

Following the 3D reconstruction of individual trees via the fused and Denoise_GAN-enhanced point clouds, key dendrometric and structural features were directly measured within the unified, georeferenced coordinate system. These included DBH in cm, DRC in cm, Tree height (in m), Lower crown height (in m), Total tree height (in m) and Crown diameter (in m). These measurements leveraged the spatially accurate and structurally refined 3D models generated by the integrated above- and below-canopy photogrammetric workflow and subsequent enhancement process (Ghasemi et al., 2025).

2.5. Detection of Stem Decline Symptoms from Below-Canopy UAV Data

2.5.1. Rationale for image-based symptom detection

Quantifying tree decline requires detection of fine-scale morphological symptoms on stems and branches, including bark lesions, woodpecker cavities, rosiness exudates, and branch breakage scars. These features manifest as textural and chromatic anomalies (Pontius and Hallett, 2014) that are spectrally resolvable by RGB imagery but fundamentally inaccessible to LiDAR due to its lack of spectral information (Cao et al., 2019). This inherent limitation of LiDAR for diagnosing biotic/abiotic stress signatures establishes the critical advantage of UAV-derived imagery for decline assessment in semi-arid forests.

2.5.2. Stem image extraction & dataset construction

Individual stems were localized within below-canopy video frames using the photogrammetric texture map ("heat map") generated during Agisoft Metashape point cloud reconstruction (Section 2.3). This texture atlas inherently associates 3D points with originating 2D imagery, enabling precise stem facet extraction. Manually annotated bounding boxes (Pascal VOC XML format) classified stems as "Declined" (N=166; exhibiting more than 1 visual symptom) or "Healthy" (N=133; no visible symptoms). Extracted 224×224 px patches underwent min-max normalization ($I' = (I - I_{min})/(I_{max} - I_{min})$) and constituted a balanced dataset for model development.

2.5.3. MobileNetV2 classifier architecture and training

We implemented a binary classifier using MobileNetV2 (Sandler, 2018), selected for its parameter efficiency (inverted residual bottlenecks with linear bottlenecks) and suitability for embedded deployment (e.g. future UAV-based real-time processing). The model was initialized with ImageNet weights. The classification head was replaced with:

1.Global Average Pooling (GAP) layer:

$$f_{GAP}: \mathbb{R}^{H\times W\times C} \rightarrow \mathbb{R} \quad (1)$$

2.Fully Connected (FC) layer (2 units) with Softmax activation:

$$P(Class=k)=\frac{exp(Z_k)}{\sum_{i=1}^{2} exp(Z_i)} \quad (2)$$

Model training used Tensor Flow 2.8 with categorical cross-entropy loss:

$$\mathscr{L} = \frac{1}{N}\sum_{i=1}^{N}\sum_{k=1}^{2} y_{i;k}\, log(p_{i;k}) \quad (3)$$

where $y_{i,k}$ is the binary indicator (0 or 1) for class k of sample i, and $p_{i,k}$ is the predicted probability.

2.6. Quantification of Crown Transparency

Crown transparency, a critical indicator of tree vitality and decline severity (Finch et al., 2021), was quantified using a 3D ray marching algorithm applied to the enhanced point clouds of individual trees. This technique simulates light penetration through the canopy by casting virtual rays from predefined origin points uniformly distributed across a hemispherical dome enveloping the crown. For each ray, the algorithm calculated the proportion of unobstructed path length (L_u) relative to total ray length within the crown volume (L_t) using the fundamental gap fraction principle:

$$\text{Transparency}(\%) = \frac{1}{N} \times \sum \frac{L_u}{L_t} \times 100 \quad (4)$$

where N is total rays cast per tree (typically 10^4-10^5). The implementation processed XYZ coordinates of crown points through the following computational workflow:

1. Crown delinitation: A minimal convex hull defined the crown volume.
2. Ray origin sampling: Uniformly distributed origins on a 2R-radius hemisphere (R = crown radius).
3. Ray propagation: Directional vectors cast toward the crown centroid with adaptive step size (δ = mean point spacing).
4. Intersection detection: At each step, points within distance threshold (d_t=3×point density) were considered obstructions.
5. Path integration: L_u accumulated during traversed gaps; L_t summed during crown occupancy.

This novel application of ray marching to UAV-derived point clouds overcomes limitations of 2D photographic methods by accounting for 3D canopy architecture, eliminating perspective distortion, enabling standardized comparison across irregular crowns, providing physical interpretation as light transmission probability.

2.7. Percentage of Tree Crown Decline

The initial photogrammetric block of the test sites was processed to generate a high-resolution orthophoto with minimal geometric distortion, ensuring spatial accuracy for subsequent analysis (Góraj et al., 2019). Individual tree crowns were manually delineated using method that was previously and exclusively introduced for Zagros forests (Ghasemi et al., 2022). The orthophoto's RGB bands were then converted to grayscale using the luminance formula:

$$\text{Gray}=0.299R+0.587G+0.114B, \quad (5)$$

standardizing intensity values while preserving textural information critical for crown health assessment (Conners and Harlow, 1980).

For each delineated crown, a localized Gray-Level Co-occurrence Matrix (GLCM) was computed within a sliding 15×15-pixel window, chosen to balance spatial detail and computational efficiency (Haralick et al., 1973). The GLCM quantified the spatial distribution of gray-level relationships by calculating the frequency of pixel intensity pairs at a fixed offset (distance = 1 pixel, angle = 0°). From the normalized GLCM, the Entropy texture index was derived as:

$$\text{Entropy}=\sum\sum P_{i,j}\, \text{log}\, P_{i,j} \quad (6)$$

where $P_{i,j}$ represents the probability of co-occurring gray levels i and j, and N is the quantization level (256). Entropy measures the randomness of textural patterns, with higher values indicating greater disorder, a property strongly correlated with crown decline. In forest health contexts, declining crowns exhibit fragmented foliage, dead branches, and irregular gaps, increasing textural heterogeneity and thus Entropy values (Bourgoin et al., 2020).

The Entropy index was linearly rescaled (0–100%) to represent the percentage of crown decline per tree. This approach is grounded in empirical evidence linking entropy to biotic stress: healthy crowns with uniform foliage yield low entropy due to structural homogeneity, while declining crowns generate high entropy from chaotic textural patterns. Validation studies confirm Entropy's sensitivity to canopy gaps and decline (Ghasemi et al., 2023), making it a robust metric for quantifying decline severity. All computations were automated using Python's scikit-image library, ensuring reproducibility.

2.8. Quantification of Tree Decline Indices

Tree decline severity was quantified using two complementary indices PDI and DAI, both implemented in the pdi R package (Finch et al., 2021). We optimized descriptors for Zagros oak ecosystems. These indices integrate the structural and symptomatic variables detailed in Table 2.

PDI computes relative decline status (0-1 scale) by ranking trees against the population percentile distribution, where higher values indicate greater decline. DAI calculates the acuteness of decline, with values between -1 to 1 indicating trends in tree decline (Finch et al., 2021).

Table 2. Structural and symptomatic variables used to estimate oak decline indices in Zagros forests.

Variable Name	Abbreviation	Units / Format	Details
Crown Transparency	--	%	Section 3.5
Stem Decline Presence	--	Binary (1/0)	Section 2.5
Diameter at Breast Height	DBH	cm	--

Diameter at Root Collar	DRC	cm	--
Total Tree Height	Height	m	--
Lower Crown Height	LCH	m	--
Crown Diameter	CD	m	Average of N-S and E-W axes
Height-to-DBH Ratio	HDR	Dimensionless	Height / DBH
Crown Projection Area	CPA	m^2	$\pi * (CD/2)^2$
Crown Volume	CV	m^3	3D model

Variable impact direction was explicitly defined. Then the applied routine within the pdi package automatically inverts rankings for negative indicators during PDI calculation. All variables received equal weighting, consistent with the ecology of Zagros forests, where no single parameter dominates decline expression (Ghasemi et al., 2024). At the end the decision tree from Finch's algorithm directly used for decline indexes calculation.

3. Result

3.1. Validation of MobileNetV2 Classifier

A key step in the development of the PDI and DAI involved the classification of tree stem condition (healthy vs. declined) using RGB video frames acquired from below the canopy. The model was trained and evaluated using 10-fold cross-validation on a dataset consisting of 166 declined stems and 133 healthy stems. The resulting confusion matrix (Figure 2) shows true positives (declined): 166, false positives: 9, false negatives: 11, and true negatives (healthy): 133. Based on this confusion matrix, the model's performance was quantified yielding overall accuracy of 96.3% and an F1-score of 0.94.

These results highlight both the effectiveness of MobileNetV2 for resource-constrained applications and the diagnostic potential of RGB imagery for detecting health-related phenotypic symptoms. Importantly, the high accuracy obtained using a lightweight network and consumer-grade imagery supports the scalability and practical implementation of this method in large-scale forest health assessments. This efficient and accessible approach enabled accurate PDI and DAI computation, further validating the strength of the proposed UAV-based decline monitoring framework.

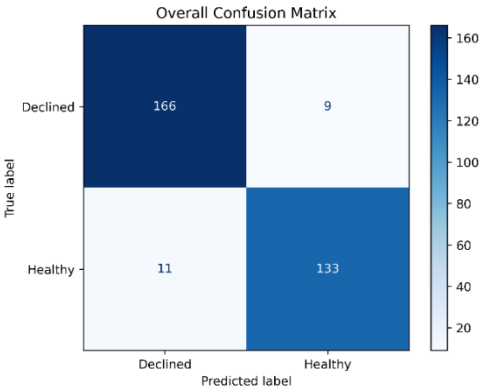

Figure 2. Confusion matrix of Declined or Healthy stems.

3.2. Trends of Oak Decline and UAV-Based phenotypic Indices

To evaluate the progression of oak decline, we compared field-assigned visual decline classes from 2018, 2019, and 2020 with the UAV-derived PDI calculated in 2024. Figure 3 illustrates a Sankey diagram that visualizes the temporal transition of individual trees among decline classes (1 to 4) across the three reference years, alongside their final PDI-based condition from our UAV analysis.

Each stream in the Sankey plot represents the trajectory of a tree health status over time, based on expert field assessments. Notably, trees originally classified as Class 1 (healthy) in 2018 showed diverse transitions: some remained healthy in 2019 and 2020, while others progressed towards Classes 2, 3, or even 4 by 2020, indicating a worsening condition. The UAV-derived PDI values from 2024, appended at the end of each stream, demonstrate strong correspondence with these multi-year field-based trajectories.

For example, trees with consistently high decline classes (e.g. remaining in Class 3 or 4 across years) show significantly elevated PDI values in 2024, validating the sensitivity of the PDI metric to long-term canopy deterioration. Conversely, trees that fluctuated or improved in class over time exhibit intermediate PDI scores, suggesting that the UAV-based phenotypic analysis captures nuanced changes in tree vitality.

This integration of historical visual classifications with advanced remote sensing metrics emphasizes the robustness of UAV-derived phenotypic indicators like PDI in reflecting multi-year decline patterns. The Sankey visualization effectively highlighted how decline dynamics, previously assessed through field observation, are traceable and quantifiable through automated, image-based analysis.

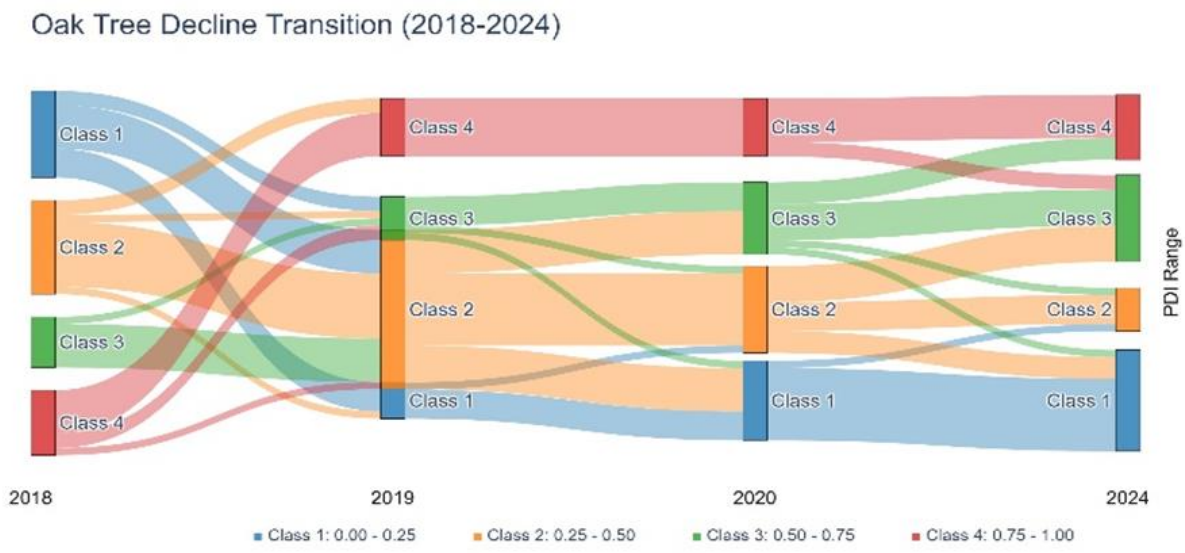

Figure 3. Decline severity during 3 years of field data collection followed by PDI in 2024.

3.3. Evaluation of DAI vs. multi-year Decline Trajectories (DWVI)

To assess the reliability and interpretive value of the DAI derived exclusively from UAV-based data in 2024, we evaluated its relationship with the Directional Weighted Variability Index (DWVI), a composite temporal indicator reflecting the decline trajectory of each tree over a six-year period. DWVI was developed to incorporate both expert-assigned visual decline classes from 2018 to 2020 (standardized to a common scale) and the 2024 UAV-derived PDI. By computing sequential annual differences in decline classes and integrating the PDI, DWVI captures both the direction and magnitude of long-term decline for each tree.

The DWVI was derived to quantify directional trends in tree health decline by integrating multi-year decline class assessments (2018–2020) and the 2024 PDI. Decline classes (1–4, representing minimal to severe deterioration) were

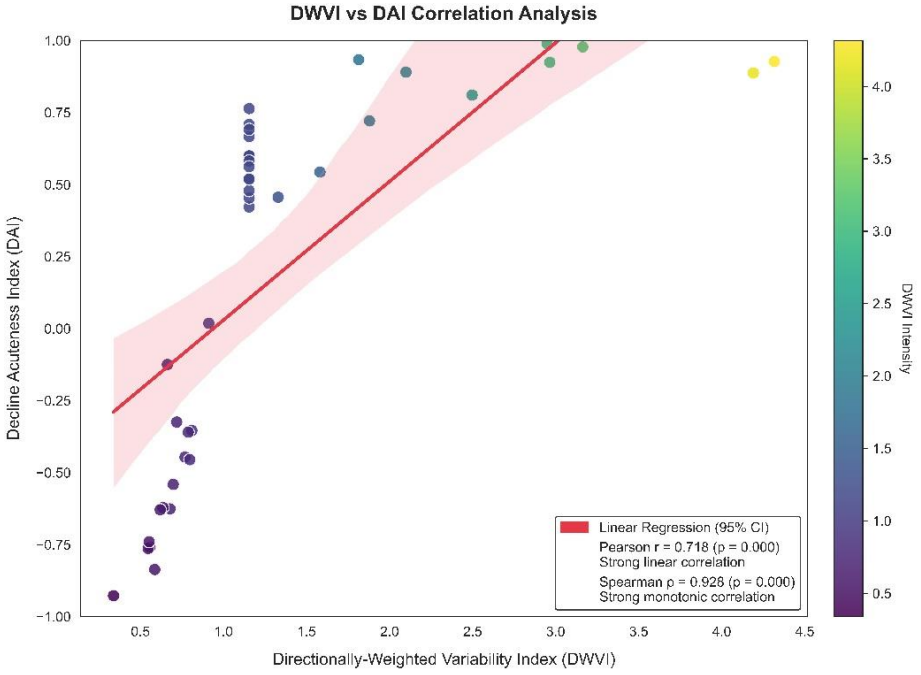

Figure 4. DAI vs. DWVI correlation

standardized, and sequential annual differences were computed to identify deterioration trajectories (e.g., class increases). The PDI (2024) was incorporated to anchor recent physiological stress. The DWVI formula prioritizes decline persistence through weighted variance:

$$\mathrm{DWVI} = \sqrt{\frac{\sum_{t=2018}^{2020}[w_t(\Delta \mathrm{Class}_t)^2]+\gamma(\mathrm{PDI}_2)^2}{n}} \quad (7)$$

where ΔClasst is the annual decline class difference (penalized if ΔClasst>0), w_t up weights deterioration years (e.g., w_t=1.5 if ΔClasst>0, else 1), and γ scales the PDI contribution.

The resulting scatter plot (Figure 4) shows the correlation between DAI (2024) and DWVI (2018–2024). A best-fit linear regression line and its 95% confidence interval are overlaid on the data. The analysis revealed a strong and statistically significant association between DAI and DWVI,

with a Pearson correlation coefficient of 0.718 and a Spearman rank correlation of 0.928. This high correlation, particularly the near-monotonic rank-based relationship, indicates that trees identified as structurally and phenotypically declined by DAI in 2024 also exhibited consistent or increasing decline patterns over previous years as captured by DWVI.

These results validate the stability, robustness, and retrospective consistency of the DAI methodology developed in this study. Despite being computed from a single temporal snapshot (2024), DAI aligns strongly with long-term field-based observations and UAV-derived phenotypic trends, confirming its suitability as a standalone indicator of oak tree health status and long-term decline.

4. Discussion

This study presents a novel, integrated UAV-based framework for high-resolution assessment of tree decline, utilizing a dual-layer flight strategy that leverages cost-effective RGB sensors. Our approach overcomes limitations of conventional aerial photogrammetry and terrestrial LiDAR by capturing both above- and below-canopy imagery to generate enhanced 3D reconstructions of individual trees. These reconstructions support the extraction of structural metrics (e.g. DBH, DRC, tree height, crown dimensions) as well as the derivation of novel phenotypic decline indicators.

The successful integration of low-cost RGB video from below the canopy makes a key advancement over existing UAV and LiDAR-based approaches. LiDAR, while powerful in capturing structural traits (e.g. crown volume, canopy height), is limited in detecting visible symptoms of decline such as bark peeling, fungal growth, and insect damage. In contrast, our below-canopy imaging method captures these visual signs directly, enabling automated detection via deep learning. The deployment of MobileNetV2, a lightweight yet robust classifier, further enhances the operational practicality of this workflow, demonstrating high classification accuracy (F1-score > 0.94) using modest computational resources.

Our approach calculates the PDI and DAI as continuous variables, providing a quantitative scale of tree health rather than coarse categorical classes. This continuous modelling enables detection of subtle decline patterns and facilitates integration with long-term monitoring data. As confirmed by Finch (2021), continuous indices provide a more nuanced and statistically powerful means of phenotyping than ordinal scores. Our findings further validate this concept: both PDI and DAI showed strong correlation with historical decline trajectories (DWVI), reinforcing their sensitivity to both structural damage and physiological stress.

The proposed workflow also offers clear operational advantages. All data acquisition was performed using widely available consumer-grade UAVs and RGB cameras, significantly reducing cost and logistical complexity compared to UAV-LiDAR or terrestrial laser scanning methods (Torresan, 2020). Moreover, the computational methods, SfM, 3D ray marching, deep learning-based classification, and PDI/DAI calculation are accessible through open-source libraries and can be executed by non-expert operators following basic training.

Given these advantages, the proposed workflow offers a scalable and repeatable solution for regional monitoring of oak decline in semi-arid forests such as Zagros. Its compatibility with autonomous UAV navigation trajectories opens possibilities for automating below-canopy data collection, improving consistency, and enabling more frequent surveys.

In summary, our method provides a cost-effective, high-resolution, and biologically meaningful system for phenotyping oak decline. It enables multi-scale analysis of structural and symptomatic indicators using only RGB imagery, contributing a practical and validated workflow for operational forest health monitoring.

5. Conclusion

This study presents a comprehensive and practical UAV-based framework for monitoring tree decline in the Zagros forests, leveraging a dual-flight strategy that integrates above-canopy and below-canopy RGB imagery. By processing these data through a photogrammetric pipeline and enhancing the resulting point clouds, we generated complete 3D models of individual trees. Structural features such as DBH, crown radius, and height were measured alongside novel indicators like crown transparency and visual decline signs detected from stem images. These metrics enabled the calculation of the PDI and DAI, offering detailed, continuous assessments of decline severity at the tree level.

Our approach demonstrates significant advantages over traditional methods by using affordable, widely available sensors and lightweight deep learning models such as MobileNetV2. The strong correlation between the UAV-derived indices and historical field-based decline assessments confirmed the reliability of our method.

Furthermore, the use of visual information from below the canopy, unavailable to LiDAR systems, enables detection of early phenotypic symptoms. The workflow's scalability, automation potential, and low-cost position it as a promising solution for routine forest health monitoring in data-scarce and ecologically sensitive regions such as Zagros forests.

6. Acknowledgements

This research was conducted within the Research Lab "Remote Sensing for Ecology and Ecosystem Conservation (RSEEC)" of the K. N. Toosi University of Technology. This research is based upon a postdoc project funded by Iran National Science Foundation (INSF) under project No.4028916.

References

Bourgoin, C., Betbeder, J., Couteron, P., Blanc, L., Dessard, H., Oszwald, J., Le Roux, R., Cornu, G., Reymondin, L., and Mazzei, L. (2020). UAV-based canopy textures assess changes in forest structure from long-term degradation. *Ecological Indicators*, 115, 106386. https://doi.org/10.1016/j.ecolind.2020.106386

Chaharmahal and Bakhtiari Administration. (n.d.). Meteorological data for Chaharmahal and Bakhtiari Province. Retrieved [May 5, 2025], from https://chbmet.ir.

Cao, L., Liu, H., Fu, X., Zhang, Z., Shen, X., and Ruan, H. (2019). Comparison of UAV LiDAR and digital aerial photogrammetry point clouds for estimating forest structural attributes in subtropical planted forests. *Forests*, 10, 145. https://doi.org/10.3390/f10020145

Conners, R. W. and Harlow, C. A. (1980). A theoretical comparison of texture algorithms, *IEEE transactions on pattern analysis and machine intelligence*, 204-222. https://doi.org/10.1109/TPAMI.1980.4767008

Dash, J. P., Watt, M. S., Pearse, G. D., Heaphy, M., and Dungey, H. S. (2017). Assessing very high resolution UAV imagery for monitoring forest health during a simulated disease outbreak, *ISPRS Journal of Photogrammetry and Remote Sensing*, 131, 1-14. https://doi.org/10.1016/j.isprsjprs.2017.07.007

Fekry, R., Yao, W., Cao, L., and Shen, X. (2022). Ground-based/UAV-LiDAR data fusion for quantitative structure modeling and tree parameter retrieval in subtropical planted forest, *Forest Ecosystems*, 9, 100065. https://doi.org/10.1016/j.fecs.2022.100065

Finch, J. P., Brown, N., Beckmann, M., Denman, S., and Draper, J. (2021). Index measures for oak decline severity using phenotypic descriptors, *Forest Ecology and Management*, 485, 118948. https://doi.org/10.1016/j.foreco.2021.118948

Gallardo-Salazar, J. L., Sáenz-Romero, C., Lindig-Cisneros, R., López-Toledo, L., Blanco-García, J. A., and Endara-Agramont, Á. R. (2023). Three decades of remote sensing analysis of forest decline related to climate change: a bibliometric study, *Cuadernos de Investigación Geográfica*, 1697-9540. https://doi.org/10.18172/cig.5639

Ghasemi, M., Latifi, H., and Pourhashemi, M. (2022). A novel method for detecting and delineating coppice trees in UAV images to monitor tree decline, *Remote Sensing*, 14, 5910. https://doi.org/10.3390/rs14235910

Ghasemi, M., Latifi, H., and Pourhashemi, M. (2023). Integrating UAV and Freely Available Space-Borne Data to Describe Tree Decline Across Semi-arid Mountainous Forests, *Environmental Modeling & Assessment*, 1-20. https://doi.org/10.1007/s10666-023-09911-3

Ghasemi, M., Latifi, H., Shafeian, E., Naghavi, H., and Pourhashemi, M. (2024). A novel linear spectral unmixing-based method for tree decline monitoring by fusing UAV-RGB and optical space-borne data, *International Journal of Remote Sensing*, 45, 1079-1109. https://doi.org/10.1080/01431161.2024.2305630

Ghasemi, M., Latifi, H., Iranmanesh, Y. (2025). Geometry-based Point Cloud Fusion of Dual-Layer UAV Photogrammetry and Unsupervised Generative Adversarial Network for 3D Tree Reconstruction in Semi-Arid Forests, *Computers and Electronics in Agriculture*, 239, 11024. https://doi.org/10.1016/j.compag.2025.111024

Góraj, M., Wróblewski, C., Ciężkowski, W., Jóźwiak, J., and Chormański, J. (2019). Free water table area monitoring on wetlands using satellite and UAV orthophotomaps-Kampinos National Park case study, *Meteorology Hydrology and Water Management. Research and Operational Applications*, 7, 23-30. https://doi.org/10.26491/mhwm/95086

Haralick, R. M., Shanmugam, K., and Dinstein, I. H. (1973). Textural features for image classification, *IEEE Transactions on systems, man, and cybernetics*, 610-621. https://doi.org/10.1109/TSMC.1973.4309314

Huang, H., Li, X., and Chen, C. (2018). Individual tree crown detection and delineation from very-high-resolution UAV images based on bias field and marker-controlled watershed segmentation algorithms, *IEEE Journal of selected topics in applied earth observations and remote sensing*, 11, 2253-2262. https://doi.org/10.1109/JSTARS.2018.2830410

Imanyfar, S., Hasanlou, M., and Mirzaei Zadeh, V. (2019). Mapping oak decline through long-term analysis of time series of satellite images in the forests of Malekshahi, Iran, *International Journal of Remote Sensing*, 40, 8705-8726. https://doi.org/10.1080/01431161.2019.1620375

Mantas, V., Fonseca, L., Baltazar, E., Canhoto, J., and Abrantes, I. (2022). Detection of tree decline (Pinus pinaster Aiton) in European forests using Sentinel-2 data, *Remote Sensing*, 14, 2028. https://doi.org/10.3390/rs14092028

Meddens, A. J. H. and Hicke, J. A. (2014). Spatial and temporal patterns of Landsat-based detection of tree mortality caused by mountain pine beetle outbreak in Colorado, USA, *Forest Ecology and Management*, 322, 78-88. https://doi.org/10.1016/j.foreco.2014.02.037

Myronenko, A. and Song, X. (2010). Point set registration: Coherent point drift, *IEEE transactions on pattern analysis and machine intelligence*, 32, 2262-2275. https://doi.org/10.1109/TPAMI.2010.46

Navarro-Cerrillo, R. M., Varo-Martínez, M. Á., Acosta, C., Rodriguez, G. P., Sanchez-Cuesta, R., and Gomez, F. J. R. (2019). Integration of WorldView-2 and airborne laser scanning data to classify defoliation levels in Quercus ilex L. Dehesas affected by root rot mortality: Management implications, *Forest Ecology and Management*, 451, 117564. https://doi.org/10.1016/j.foreco.2019.117564

Olson, L. G., Coops, N. C., Moreau, G., Hamelin, R. C., and Achim, A. (2025). The assessment of individual tree canopies using drone-based intra-canopy photogrammetry, *Computers and Electronics in Agriculture*, 234, 110200. https://doi.org/10.1016/j.compag.2025.110200

Pontius, J. and Hallett, R. (2014). Comprehensive methods for earlier detection and monitoring of forest decline, *Forest Science*, 60, 1156-1163. https://doi.org/10.5849/forsci.13-121

Pourhashemi, M. and Sadeghi, S. M. M. (2020). A review on ecological causes of oak decline phenomenon in forests of Iran, *Ecology of Iranian Forest*, 8, 148-164. https://doi.org/10.52547/ifej.8.16.148

Magnuson, R., Erfanifard, Y., Kulicki, M., Gasica, T.A., Mielcarek, M., Sterenczak, K (2024). Mobile Devices in Forest Mensuration: A Review of Technologies and Methods in Single Tree Measurements, *Remote Sensing*, 16, 3570. https://doi.org/10.3390/rs16193570

Sagheb Talebi, K., Sajedi, T., and Pourhashemi, M. (2014). Forests of Iran: A Treasure from the Past, a Hope for the Future. Springer. 152p. ISBN: 978-94-007-7370-7

Sandler, M., Howard, A., Zhu, M., Zhmoginov, A., & Chen, L. C, (2018). MobileNetV2: Inverted Residuals and Linear Bottlenecks, *Proceedings of the IEEE Conference on Computer Vision and Pattern Recognition (CVPR)*, 4510–4520. https://doi.org/10.1109/CVPR.2018.00474

Torresan, C. e. a. (2020). Forestry applications of UAVs in Europe: A review, *International Journal of Remote Sensing*, 41(22), 8536–8573. https://doi.org/10.1080/01431161.2016.1252477

Wang, Y., Kukko, A., Hyyppä, E., Hakala, T., Pyörälä, J., Lehtomäki, M., El Issaoui, A., Yu, X., Kaartinen, H., and Liang, X. (2021b). Seamless integration of above- and under-canopy unmanned aerial vehicle laser scanning for forest investigation, *Forest Ecosystems*, 8, 1-15. https://doi.org/10.1186/s40663-021-00290-3

Xiang, T.-Z., Xia, G.-S., and Zhang, L. (2019). Mini-unmanned aerial vehicle-based remote sensing: Techniques, applications, and prospects, *IEEE geoscience and remote sensing magazine*, 7, 29-63. https://doi.org/10.1109/MGRS.2019.2918840

Zakeri Anaraki, S. and Fallah Shamsi, S. R. (2014). An investigation on Persian oak (Quercus brantii Lindl) single tree defoliation mapping, using Rapideye and Aster-L1B satellite imageries, *Iranian Journal of Forest*, 5, 443-456.

Zarco-Tejada, P. J., Hornero, A., Beck, P. S. A., Kattenborn, T., Kempeneers, P., and Hernández-Clemente, R. (2019). Chlorophyll content estimation in an open-canopy conifer forest with Sentinel-2A and hyperspectral imagery in the context of forest decline, *Remote Sensing of Environment*, 223, 320-335. https://doi.org/10.1016/j.rse.2019.01.031